SCIENTIFIC REPORTS
nature research

OPEN

A Jeffrey Fluid Model for a Porous-walled Channel: Application to Flat Plate Dialyzer

M. Kahshan[1,2], D. Lu[1*] & A. M. Siddiqui[3]

Creeping motion of a Jeffrey fluid in a small width porous-walled channel is presented with an application to flow in flat plate hemodialyzer. Darcy's law is used to characterize the fluid leakage through channel walls. Using suitable physical approximations, approximate analytical solution of equations of motion is obtained by employing perturbation method. Expressions for velocity field and the hydrostatic pressure are obtained. Effects of filtration coefficient, the inlet pressure and Jeffrey fluid parameters on the flow characteristics are discussed graphically. The derived results are used to study the flow of filtrate in a flat plat hemodialyzer. Using the derived solutions, theoretical values of the filtration rate and the mean pressure difference in the hemodialyzer are calculated. On comparing the computed results with the available experimental data, a reasonable agreement between the two is found. It is concluded that the presented model can be used to study the hydrodynamical aspects of the fluid flow in a flat plate hemodialyzer.

The study of hydrodynamics of fluid flow in porous-walled channels and tubes have been remained a subject of interest for researchers since decades. This is because of the occurrence of such flows in many areas of science and engineering, particularly in those processes where mass transfer and filtration are encountered. Desalination process due to reverse osmosis, transpiration cooling, ultrafiltration in the tubules of glomerulus and fluid reabsorption through permeable walls of renal proximal tubule in kidneys, and blood filtration during hemodialysis in an artificial kidney are examples of such flows[1–6]. A common characteristic of such flows is the direct inapplicability of the usual Poiseuille law[7] in these situations because of the existence of non-zero velocity components of fluid in both axial and normal directions. This happens because of the fluid leakage through porous walls of the channel.

Literature survey reveals that various researchers have attempted the problem of fluid flow in porous-walled channels and tubes[5,8–12] by assuming different forms of fluid reabsorption at the walls. Berman[8], Sellars[9], and Yuan[10] have studied the laminar flow of incompressible Newtonian fluid in a uniformly porous-walled channel. Solutions were obtained for a uniform suction or injection case using the regular perturbation method. Kozinski *et al.*[11] and Siddiqui *et al.*[12] also studied the creeping flow of a viscous fluid in a permeable channel. Exact solutions were found for the case in which the leakage has exponential and linear decaying rate along the channel length. Flow of a viscous fluid in a porous-walled channel was also studied by Marshall *et al.*[5] who assumed that the fluid leakage across the channel walls is proportional to the pressure differences across the walls. For further studies of fluid flows under different flow conditions authors would refer the reader to[13–19].

In the literature presented above, all studies were performed for the Newtonian fluid model only. Despite the fact that most of the industrial and biological fluids are non-Newtonian[20] and the classical Newton's law of viscosity fails to describe the complex rheological properties of non-Newtonian fluids, a very little work has been done in order to study the non-Newtonian fluids flow in porous-walled channels and tubes. Amongst many non-Newtonian fluid models, one is the Jeffrey fluid model that has attracted many researchers due to its consideration as a better model for physiological fluids[21–23]. The Jeffrey model is recognized as a generalization of the frequently used Newtonian fluid model because of the fact tat its constitutive equation can be reduced to that of the Newtonian model's as a special case. The Jeffrey fluid model is capable of describing the stress relaxation property of non-Newtonian fluids, which the usual viscous fluid model cannot describe. Class of non-Newtonian fluids having the characteristic memory time scale, also known as the relaxation time, can be described well by the Jeffrey fluid model. Therefore, this article is devoted to the study of an incompressible Jeffrey fluids' flow in

[1]Faculty of Science, Jiangsu University, Zhenjiang, Jiangsu, 212013, P.R. China. [2]Department of Mathematics, COMSATS University Islamabad, Abbottabad Campus, Abbottabad, 22060, Pakistan. [3]Pennsylvania State University, York Campus, Edgecomb, 1703, USA. *email: dclu@ujs.edu.cn

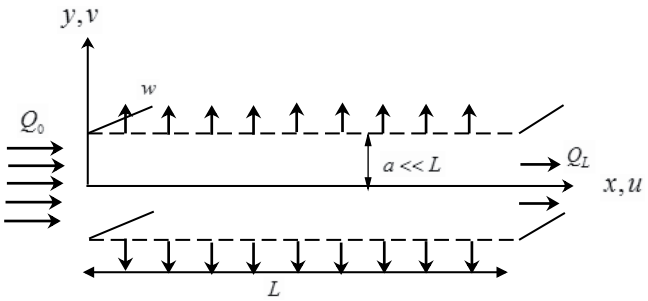

Figure 1. Geometry of the flow.

a porous-walled channel of small width. Fluid absorption at the channel wall is taken in accordance with the Darcy's law. The approach of the present analysis seems better from that of[2,3,11,24]. In the present approach, the fluid loss at the wall is taken as function of the wall permeability, the flow rate then determined can be found to decay linearly or exponentially along the channel wall as special case in our study. Whereas, in[2,3,11,24] a flow rate that decays linearly or exponentially, along the channel and tube was assumed in advance.

Problem Formulation

Let us consider the steady and creeping motion of an incompressible Jeffrey fluid in a porous-walled channel comprising of two equidistant parallel flat plates of length L distance $2a$ apart. A Cartesian coordinate system $(\tilde{x}, \tilde{y})$ is chosen in a such that the axis of symmetry lies at $y = 0$ as shown in Fig. 1. It is assumed that the fluid moves only due to the hydrostatic pressure. Hydrostatic and osmotic pressures outside the channel are also assumed ot be constant. The flow is governed by the following equations

$$\frac{\partial \tilde{p}}{\partial \tilde{x}} = \frac{\partial}{\partial \tilde{x}}(\tilde{S}_{\tilde{x}\tilde{x}}) + \frac{\partial}{\partial \tilde{y}}(\tilde{S}_{\tilde{x}\tilde{y}}), \tag{1}$$

$$\frac{\partial \tilde{p}}{\partial \tilde{y}} = \frac{\partial}{\partial \tilde{x}}\left(\tilde{S}_{\tilde{y}\tilde{x}}\right) + \frac{\partial}{\partial \tilde{y}}\left(\tilde{S}_{\tilde{y}\tilde{y}}\right), \tag{2}$$

$$\frac{\partial \tilde{u}}{\partial \tilde{x}} + \frac{\partial \tilde{v}}{\partial \tilde{y}} = 0, \tag{3}$$

where $\tilde{p}$ is the hydrostatic pressure of the fluid, $\tilde{S}_{ij}$, $i, j = \tilde{x}, \tilde{y}$ are components of the extra stress tensor, $\tilde{u}$ and $\tilde{v}$ are components of the velocity vector $\tilde{\mathbf{V}}(\tilde{x}, \tilde{y})$ in the axial and transverse directions, respectively.

The extra stress tensor $\tilde{S}$ for the Jeffrey fluid is given by the following equation[21–23]

$$\tilde{\mathbf{S}} = \frac{\mu}{1 + \lambda_1}[\dot{\mathbf{A}} + \tilde{\lambda_2}\ddot{\mathbf{A}}], \tag{4}$$

where μ is the dynamic viscosity of the fluid, $\dot{\mathbf{A}}$ is the shear rate, $\tilde{\lambda_2}$ is the retardation time, λ_1 is the ratio of relaxation time to the retardation time, and $\ddot{\mathbf{A}}$ represents differentiation of $\dot{\mathbf{A}}$. The initial and boundary conditions corresponding to the prescribed flow are

$$\tilde{v}(\tilde{x}, 0) = 0, \tag{5}$$

$$\partial \tilde{u}(\tilde{x}, 0)/\partial \tilde{y} = 0, \tag{6}$$

$$\tilde{v}(\tilde{x}, a) = \frac{L_p}{\mu t}[\tilde{p}(\tilde{x}, a) - p_m], \tag{7}$$

$$\tilde{u}(\tilde{x}, a) = 0, \tag{8}$$

$$\frac{1}{a}\int_0^a \tilde{p}(0, \tilde{y})d\tilde{y} = \tilde{p}_i, \tag{9}$$

$$2w\int_0^a \tilde{u}(0, \tilde{y})d\tilde{y} = \tilde{Q}_i. \tag{10}$$

Equations (5) and (6) are the symmetry conditions at the center line of the channel. Equation (7) is the consequence of the Darcy's law at the permeable wall of the channel, where L_p is the mechanical filtration coefficient of

the channel wall which is usually measured in the units of $cm^2(L_p/\mu t$ is called the hydraulic permeability of the channel wall), t is the wall thickness, and p_m can be visualized as the back pressure that opposes the fluid leakage and it is equal to the difference of hydrostatic and the osmotic pressures outside the channel wall. Equation (8) is the no slip condition at the wall, whereas Equations (9 and 10) are the inlet conditions. In these equations $\widetilde{p}_i$ is the mean pressure and $\widetilde{Q}_i$ is the flow rate at the inlet of the channel at $\widetilde{x} = 0$.

Dimensionless Formulation

Following parameters are used to transform equations into dimensionless form:

$$x = \frac{\widetilde{x}}{L};\ y = \frac{\widetilde{y}}{a};\ u(x, y) = \frac{a^2\widetilde{u}}{\widetilde{Q}_i};\ v(x, y) = \frac{aL\widetilde{v}}{\widetilde{Q}_i}. \tag{11}$$

Using the above quantities, Eqs (1−3) take the following form

$$\frac{\partial p}{\partial x} = \delta\frac{\partial}{\partial x}(S_{xx}) + \frac{\partial}{\partial y}(S_{xy}), \tag{12}$$

$$\frac{\partial p}{\partial y} = \delta^2\frac{\partial}{\partial x}\left(S_{yx}\right) + \delta\frac{\partial}{\partial y}\left(S_{yy}\right), \tag{13}$$

$$\frac{\partial u}{\partial x} + \frac{\partial v}{\partial y} = 0, \tag{14}$$

where $\delta = \frac{a}{L}$ is the ratio of channel height to its length, $\mathbf{S} = \frac{a^3\widetilde{\mathbf{S}}}{\mu\widetilde{Q}_i}$ is the dimensional stress tensor and $p(x, y) = \frac{a^4}{\mu L\widetilde{Q}_i}[\widetilde{p}\,(\widetilde{x}, \widetilde{y}) - p_m]$. The initial and boundary conditions Eqs (5−10) are transformed into the following dimensionless form

$$v(x, 0) = 0, \tag{15}$$

$$\partial u(x, 0)/\partial x = 0, \tag{16}$$

$$v(x, 1) = Kp(x, 1), \tag{17}$$

$$u(x, 1) = 0, \tag{18}$$

$$\int_0^1 p(0, y)dy = p_i, \tag{19}$$

$$2A\int_0^1 u(0, y)dy = 1, \tag{20}$$

where $K = \frac{L_pL^2}{a^3t}$ is the dimensionless wall filtration parameter and $\lambda_2 = \frac{\widetilde{\lambda}_2\widetilde{Q}_i}{a^2L}$ is the Jeffrey fluid parameter in dimensionless form, $A = \frac{w}{a}$ is the ratio of channel width to height and $Q(x) = \frac{\widetilde{Q}(\widetilde{x})}{\widetilde{Q}_i}$.

Using Eq. (4) and the dimensionless parameters, the components of the stress tensor $\mathbf{S}$ can be readily obtained in the following dimensionless form

$$S_{xx} = \frac{2\delta}{1+\lambda_1}\left[1 + \lambda_2\left(u\frac{\partial}{\partial x} + v\frac{\partial}{\partial y}\right)\right]\left(\frac{\partial u}{\partial x}\right), \tag{21}$$

$$S_{xy} = \frac{1}{1+\lambda_1}\left[1 + \lambda_2\left(u\frac{\partial}{\partial x} + v\frac{\partial}{\partial y}\right)\right]\left(\frac{\partial u}{\partial y} + \delta^2\frac{\partial v}{\partial x}\right), \tag{22}$$

$$S_{yx} = \frac{1}{1+\lambda_1}\left[1 + \lambda_2\left(u\frac{\partial}{\partial x} + v\frac{\partial}{\partial y}\right)\right]\left(\frac{\partial u}{\partial y} + \delta^2\frac{\partial v}{\partial x}\right), \tag{23}$$

$$S_{yy} = \frac{2\delta^2}{1+\lambda_1}\left[1 + \lambda_2\left(u\frac{\partial}{\partial x} + v\frac{\partial}{\partial y}\right)\right]\left(\frac{\partial v}{\partial y}\right). \tag{24}$$

Description	Symbol	Numerical data
Membrane length	L	42 cm
Membrane thickness	t	2.59×10^{-3} cm
Membrane width	w	11.6 cm
Blood compartments		8
Height of the blood half channel	a	9×10^{-3} cm
Entrance trans-membrane pressure difference	$\bar{P}_0 - P_T$	150 mm Hg
Viscosity of the fluid	μ	6.9×10^{-3} dynes-sec/cm^2
Entrance volume flow rate	$8Q_0$	160 ml/min
Ultrafiltration rate	$8Q_w$	200 ml/hr

Table 1. Experimental data for the RP kidney [4,6,29].

Solution to the Problem

The set of Eqs (12−14) contains nonlinear coupled partial differential equations in three unknowns u, v and p and it is not possible to determine an exact solution of it. Since the channel is narrow and has small width as compared with its length, therefore the dimensionless parameter δ is very small. Thus it seems reasonable to ignore terms of the order δ^2 and higher order. Note that this is also true for the flat plate hemodialyzer, for which the parameter δ^2 is of the order 10^{-8} (see the data given in Table 1 and [25–27]).

Now expanding u, v and p in the power series of the dimensionless Jeffrey fluid parameter as

$$(u, v, p) = (u_0, v_0, p_0) + \lambda_2(u_1, v_1, p_1) + O(\lambda_2^2), \tag{25}$$

we obtain the following systems of initial-boundary-value problem up-to the Order (λ_2):

Zeroth order system.

$$\frac{\partial p_0}{\partial y} = 0 \tag{26}$$

$$\frac{\partial p_0}{\partial x} = \frac{1}{1 + \lambda_1}\frac{\partial^2 u_0}{\partial y^2}, \tag{27}$$

$$\frac{\partial u_0}{\partial x} + \frac{\partial v_0}{\partial y} = 0, \tag{28}$$

$$v_0(x, 0) = 0, \tag{29}$$

$$\partial u_0(x, 0)/\partial x = 0, \tag{30}$$

$$v_0(x, 1) = Kp_0(x, 1), \tag{31}$$

$$u_0(x, 1) = 0, \tag{32}$$

$$\int_0^1 p_0(0, y)dy = p_i, \tag{33}$$

$$2A\int_0^1 u_0(0, y)dy = 1. \tag{34}$$

First order system.

$$\frac{\partial p_1}{\partial y} = 0 \tag{35}$$

$$\frac{\partial p_1}{\partial x} = \frac{1}{1 + \lambda_1}\frac{\partial}{\partial y}\left[\frac{\partial u_1}{\partial y} + \left(u_0\frac{\partial}{\partial x} + v_0\frac{\partial}{\partial y}\right)\left(\frac{\partial u_0}{\partial y}\right)\right], \tag{36}$$

$$\frac{\partial u_1}{\partial x} + \frac{\partial v_1}{\partial y} = 0, \tag{37}$$

$$v_1(x, 0) = 0, \tag{38}$$

$$\partial u_1(x, 0)/\partial x = 0, \tag{39}$$

$$v_1(x, 1) = Kp_1(x, 1), \tag{40}$$

$$u_1(x, 1) = 0, \tag{41}$$

$$\int_0^1 p_1(0, y)dy = 0, \tag{42}$$

$$\int_0^1 u_1(0, y)dy = 0. \tag{43}$$

Zeroth order solution. The exact solution of the zeroth order system is given in the following

$$u_0(x, y) = \frac{1 + \lambda_1}{2}\frac{dp_0}{dx}(y^2 - 1), \tag{44}$$

$$v_0(x, y) = -\frac{1 + \lambda_1}{6}\frac{d^2p_0}{dx^2}(y^3 - 3y), \tag{45}$$

$$p_0(x) = \left(\frac{p_i}{2} + \frac{\xi}{4AK}\right)e^{-\xi x} + \left(\frac{p_i}{2} - \frac{\xi}{4AK}\right)e^{\xi x}, \tag{46}$$

where $\xi = \sqrt{\frac{3K}{1 + \lambda_1}}$.

First order solution. The exact solution of the first order system is given in the following

$$u_1(x, y) = \frac{1 + \lambda_1}{2}\frac{dp_1}{dx}(y^2 - 1) - \frac{(1 + \lambda_1)^2}{12}\frac{dp_0}{dx}\frac{d^2p_0}{dx^2}(y^4 - 1), \tag{47}$$

$$\begin{aligned} v_1(x, y) \;=\; & -\frac{1 + \lambda_1}{6}\frac{d^2p_1}{dx^2}(y^3 - 3y) \\ & + \frac{(1 + \lambda_1)^2}{60}\frac{d}{dx}\left(\frac{dp_0}{dx}\frac{d^2p_0}{dx^2}\right)(y^5 - 5y), \end{aligned} \tag{48}$$

$$p_1(x) = C_3e^{-\xi x} + C_4e^{\xi x} + \frac{2}{15}\xi^2(1 + \lambda_1)(C_1^2e^{-2\xi x} + C_2^2e^{2\xi x}), \tag{49}$$

where the constants C_1, C_2, C_3 and C_4 are respectively given by the following expressions

$$C_1 = \frac{p_i}{2} + \frac{\xi}{4AK}, \tag{50}$$

$$C_2 = \frac{p_i}{2} - \frac{\xi}{4AK}, \tag{51}$$

$$C_3 = \xi^2(1 + \lambda_1)\left[\frac{pi\xi}{20AK} + \frac{1}{15}(3C_1^2 - C_2^2)\right], \tag{52}$$

$$C_4 = \xi^2(1 + \lambda_1)\left[-\frac{pi\xi}{20AK} + \frac{1}{15}(C_1^2 - 3C_2^2)\right]. \tag{53}$$

Summing up, the approximate solution upto the order λ_2 can be readily obtained as

$$\begin{aligned} u(x, y) &= u_0(x, y) + \lambda_2 u_1(x, y), \\ &= \frac{1}{2}(1 + \lambda_1)\frac{dp}{dx}(y^2 - 1) \\ &\quad -\frac{1}{12}(1 + \lambda_1)^2\lambda_2\frac{dp_0}{dx}\frac{d^2p_0}{dx^2}(y^4 - 1). \end{aligned} \tag{54}$$

$$\begin{aligned} v(x, y) &= v_0(x, y) + \lambda_2 v_1(x, y), \\ &= -\frac{1}{6}(1 + \lambda_1)\frac{d^2p}{dx^2}(y^3 - 3y) \end{aligned} \tag{55}$$

$$+\frac{1}{60}(1 + \lambda_1)^2\lambda_2\frac{d}{dx}\left(\frac{dp_0}{dx}\frac{d^2p_0}{dx^2}\right)(y^5 - 5y). \tag{56}$$

$$\begin{aligned} p(x) &= p_0(x) + \lambda_2 p_1(x), \\ &= (C_1 + \lambda_2 C_3)e^{-\xi x} + (C_2 + \lambda_2 C_4)e^{\xi x} \\ &\quad +\frac{2}{15}\xi^2(1 + \lambda_1)\lambda_2(C_1^2e^{-2\xi x} + C_2^2e^{2\xi x}). \end{aligned} \tag{57}$$

It is remarkable to point out that in the above velocity and pressure profiles, we get contribution of both parameters λ_1 and λ_2 of the Jeffrey fluid. For the limiting case when $\lambda_1 \to 0$ and $\lambda_2 \to 0$, the presented solutions reduce to the solution for Newtonian fluid flow in a permeable channel.

Expressions for Various Quantities of Interest

The dimensionless mean pressure $\overline{p}(x)$ taken over any cross-section of the channel is defined as

$$\begin{aligned} \overline{p}(x) &= \frac{1}{2}\int_{-1}^{1} p(x, y)dy \\ &= p(x) \end{aligned}$$

Hence the difference of mean pressure $\Delta p(x)$ can be obtained as

$$\begin{aligned} \Delta p(x) &= \overline{p}(0) - \overline{p}(x), \\ &= p_i - (C_1 + \lambda_2 C_3)e^{-\xi x} - (C_2 + \lambda_2 C_4)e^{\xi x} \\ &\quad -\frac{2}{15}\xi^2(1 + \lambda_1)\lambda_2(C_1^2e^{-2\xi x} + C_2^2e^{2\xi x}). \end{aligned} \tag{58}$$

The non-dimensional wall shear stress may be obtained as

$$\begin{aligned} \tau_w(x) &= -S_{yx}|_{y=1}, \\ &= -\frac{1}{(1 + \lambda_1)}\left[\frac{\partial u}{\partial y} + \lambda_2\left(u_0\frac{\partial^2 u_0}{\partial x \partial y} + v_0\frac{\partial^2 u_0}{\partial y^2}\right)\right]_{y=1}. \end{aligned} \tag{59}$$

The dimensionless volume flow rate at any cross-section of the channel can be computed as

$$\begin{aligned} Q(x) &= A\int_{-1}^{1} u(x, y)dy \\ &= -\frac{2}{3}A(1 + \lambda_1)\left[\frac{dp}{dx} - \frac{1}{5}\lambda_2(1 + \lambda_1)\frac{dp_0}{dx}\frac{d^2p_0}{dx^2}\right]. \end{aligned} \tag{60}$$

The expression for leakage flux $q(x)$ can be readily obtained as following

$$\begin{aligned} q(x) &= -\frac{dQ}{dx}, \\ &= \frac{2}{3}A(1 + \lambda_1)\left[\frac{d^2p}{dx^2} - \frac{1}{10}\lambda_2(1 + \lambda_1)\frac{d^2}{dx^2}\left(\frac{dp_0}{dx}\right)^2\right]. \end{aligned} \tag{61}$$

The fractional re-absorption (FR) is the amount of fluid that has been reabsorbed through the channel walls. It can be computed using the following expression

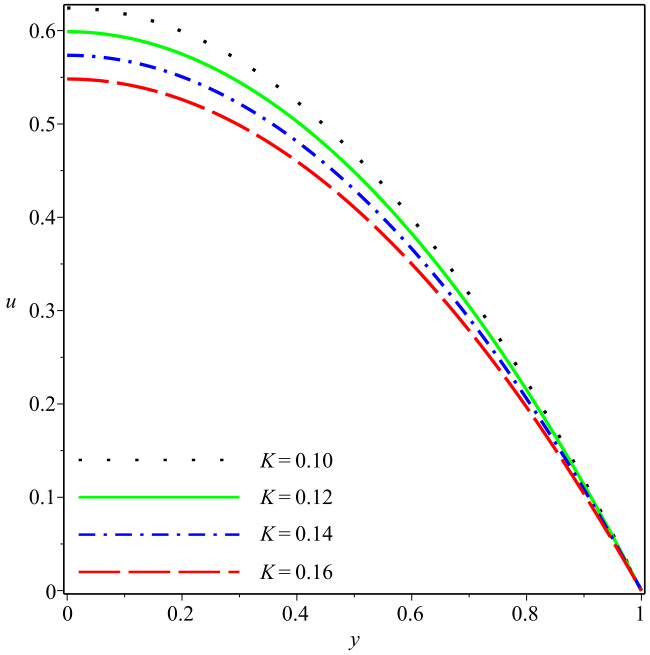

Figure 2. Effect of K on the axial velocity for $p_i = 3$, $\lambda_1 = 0.1$, $\lambda_2 = 0.03$.

$$FR = \frac{Q(0) - Q(1)}{Q(0)}. \tag{62}$$

The streamlines can be determined by using the following relation

$$\frac{dx}{u} = \frac{dy}{v}. \tag{63}$$

Thus streamlines can be obtained up to the order λ_2 by the following equation

$$10\frac{dp}{dx}(y^3 - 3y) - \lambda_2(1 + \lambda_1)\frac{dp_0}{dx}\frac{d^2p_0}{dx^2}(y^5 - 5y) = C_5, \tag{64}$$

where C_5 is an arbitrary constant.

Results and Discussion

This section describes effects of the inlet pressure p_i, wall permeability parameter K and the Jeffrey fluid parameters λ_1 and λ_2 on the axial and normal velocity components $u(x, y)$, $v(x, y)$, the mean pressure difference $\Delta p(x)$ and the streamline patterns.

Figures 2–5 present the variation of $u(x, y)$ with y at the cross-section $x = 0.3$ of the channel for different values of K, p_i, λ_1 and λ_2, respectively. A parabolic axial velocity is formed that has the maximum value at the center line of channel and is zero at the boundary. These figures reveal that the magnitude of axial velocity decreases rapidly as the inlet pressure and the wall permeability are increased. Similar effects are also noticed when the magnitudes of Jeffery fluid parameters is increased. However relatively small variations happen due to increase of λ_1 and λ_2 as compared to those due to p_i and K.

Figures 6–9 present the variation of $v(x, y)$ with y at the cross-section $x = 0.3$ of the channel for different values of K, p_i, λ_1 and λ_2, respectively. Comparing with the axial velocity distribution, opposite effects of these parameters are observed on the normal velocity component. It can be seen clearly that v increases rapidly as the magnitudes of p_i, K, λ_1 and λ_2 are increased. Thus, the wall seepage enhances by increasing these parameters. Effect of λ_1 and λ_2 on v are prominent as compared to those on u.

Variations of the mean pressure difference in the axial direction for different values of p_i, K, λ_1 and λ_2 are shown in Figs 10–13. These figures depict that Δp decreases rapidly as the values of these parameters are increased. It can also be seen that variations in Δp are dominant after the middle of the channel.

Streamline pattern of the flow is presented in Figs 14–17. It is observed from the Fig. 14 that the flow is positive axial through the length of channel and no reverse flow and reverse leakage occurs for prescribed values of the parameters. However, as the wall permeability parameter K and (or) the inlet pressure p_i increase to a certain value, a reverse flow phenomenon occurs. It happens due to the fact that if K or p_i are increased, all the entering fluid is reabsorbed through seepage at the channel wall before the channel exit. Thus, a stagnation point flow can

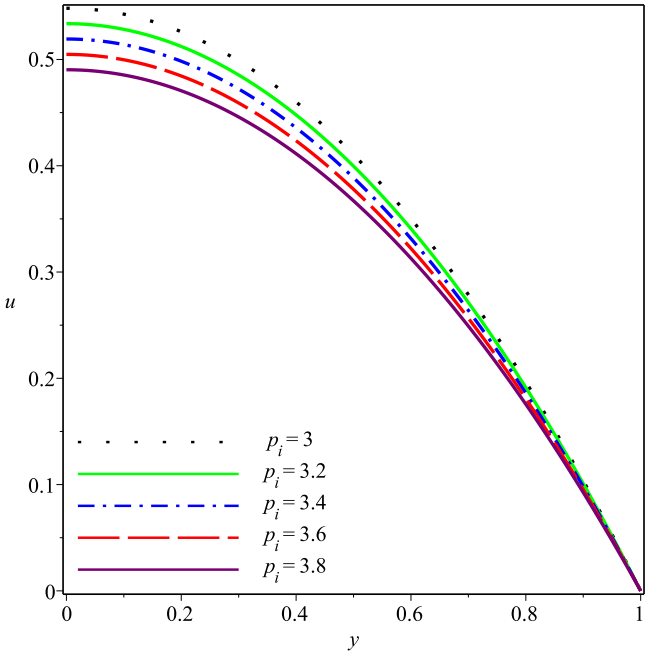

Figure 3. Effect of p_i on the axial velocity for $K = 0.16$, $\lambda_1 = 0.1$, $\lambda_2 = 0.03$.

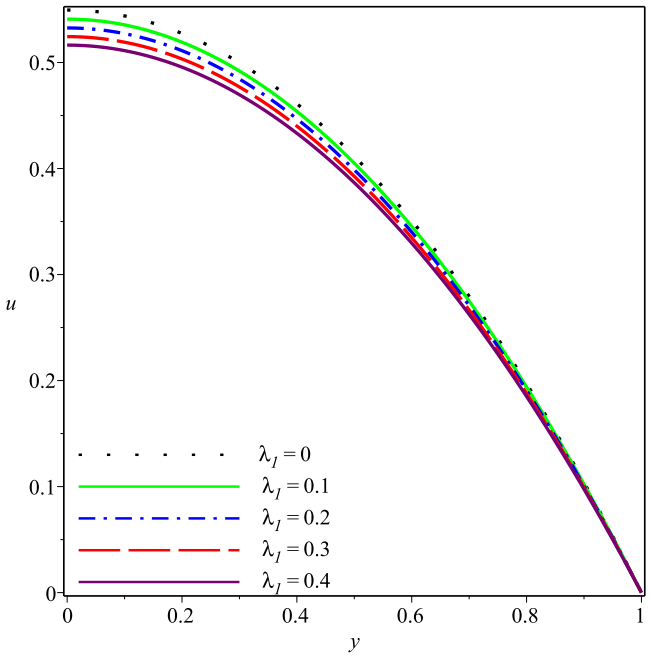

Figure 4. Effect of $\lambda 1$ on the axial velocity for $p_i = 3$, $K = 0.16$, $\lambda_2 = 0.03$.

be seen in these two figures, Figs 15 and 16. A comparison of Figs 14 and 17 show that a very nominal increase in the fluid seepage through channel walls happen as the value of λ_1 is increased.

Application to Flat Plate Hemodialyzer

In this section, we aim to derive equations for the computation of ultrafiltration rate Q_A and the mean pressure drop ΔP in an artificial kidney (FPD) by using results of the former section. An FPD comprises of several compartments of blood. Every compartment involves two rectangular sheets that are composed of recovered cellulose. The two sheets are clipped at their edges by a couple of rectangular notched plastic sheets. The blood streams between the cellulose sheets whereas the dializing liquid goes in a counter-current or a cross-current stream along the sections in hemodialyzer board[6,27–29]. The volume of blood lost by the leakage through cellulose in a given time, from a known recycling volume is taken to be the ultrafiltration rate.

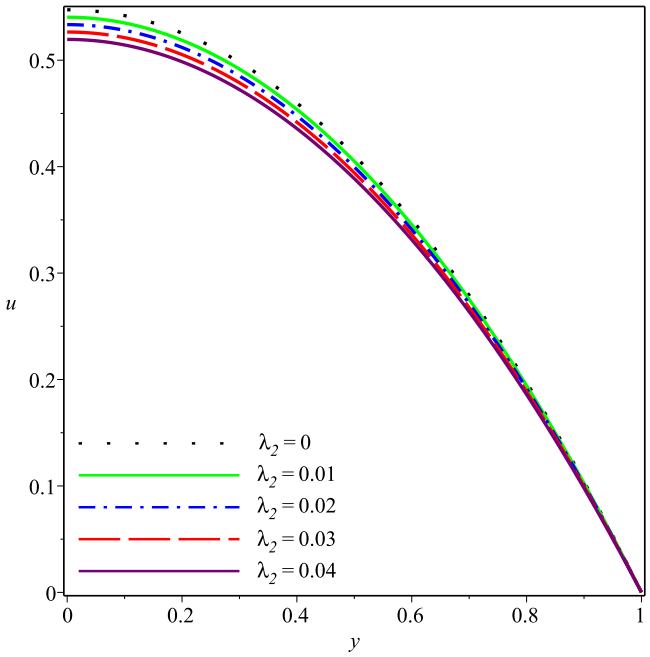

Figure 5. Effect of λ_2 on the axial velocity for $p_i = 3$, $K = 0.16$, $\lambda_1 = 0.1$.

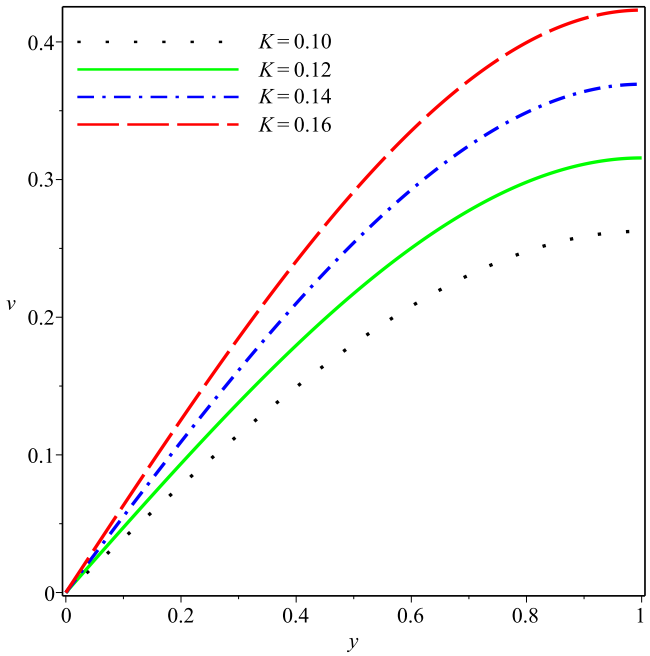

Figure 6. Effect of K on the normal velocity for $p_i = 3$, $\lambda_1 = 0.1$, $\lambda_2 = 0.03$.

Let L be the cellulose length, then we can compute the ultrafiltration rate for the presented model as following

$$\widetilde{Q}_A = \widetilde{Q}_0 - \widetilde{Q}_L, \tag{65}$$

where sign denotes the dimensional quantity, $Q_0 = Q(0)$ and $Q_L = Q(L)$. The non-dimensional expression for $\widetilde{Q}_A$ can be obtained using the dimensionless parameters defined earlier. Making use of (46), (49) and (60) in (65), the following expression for the ultrafiltration rate is determined

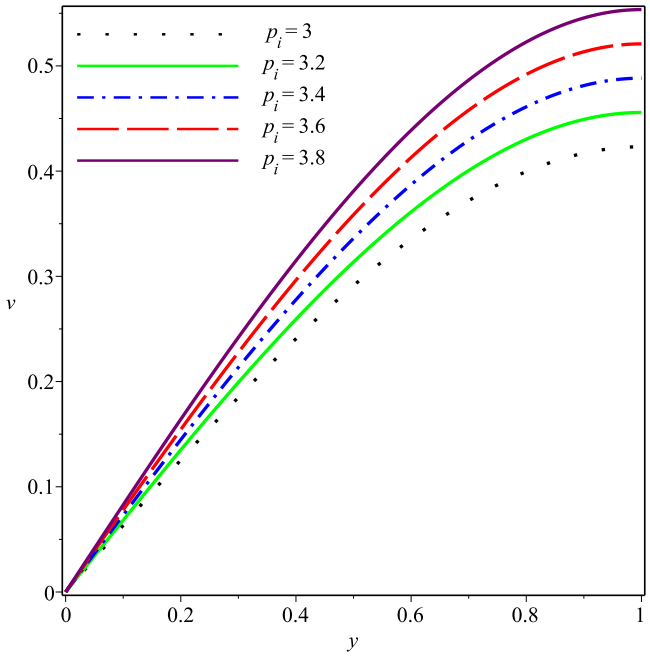

Figure 7. Effect of p_i on the normal velocity for $K = 0.16$, $\lambda_1 = 0.1$, $\lambda_2 = 0.03$.

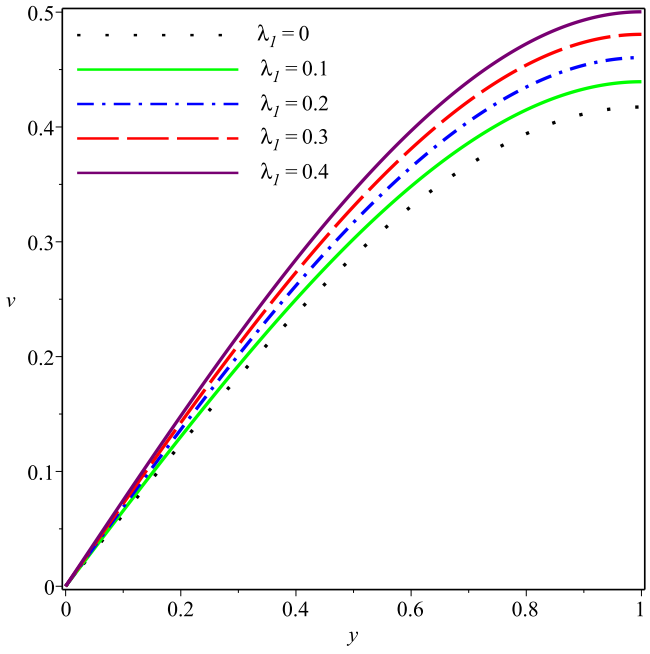

Figure 8. Effect of λ_1 on the normal velocity for $p_i = 3$, $K = 0.16$, $\lambda_2 = 0.03$.

$$\begin{aligned} Q_A &= Q_0 - Q_1, \\ &= 1 - \frac{1}{5}(5 - \lambda_2 K p_i)\cosh\xi - \frac{1}{5}\lambda_2 K p_i \cosh 2\xi \\ &\quad - \frac{\xi}{30A}[3\lambda_2 + (4A^2 K p_i^2 \lambda_2 - 20A^2 p_i)(1 + \lambda_1)]\sinh\xi \\ &\quad + \frac{\xi\lambda_2}{60A}[3 + 4A^2 K p_i^2 (1 + \lambda_1)]\sinh 2\xi. \end{aligned} \tag{66}$$

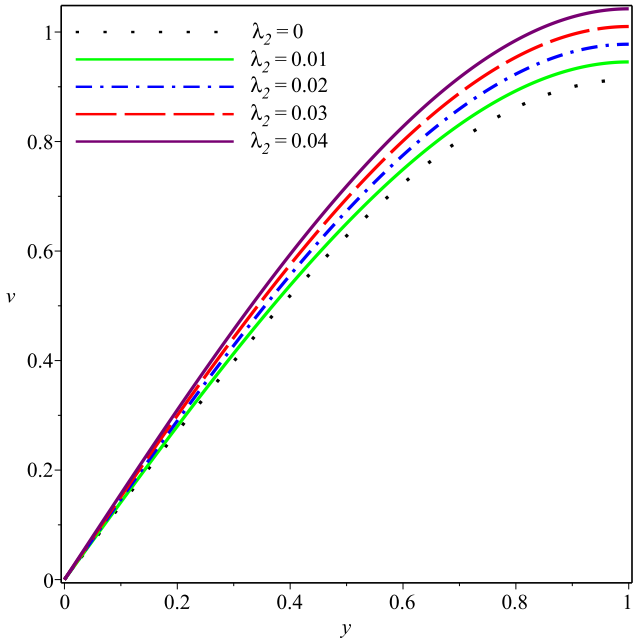

Figure 9. Effect of λ_2 on the normal velocity for $p_i = 3$, $K = 0.16$, $\lambda_1 = 0.1$.

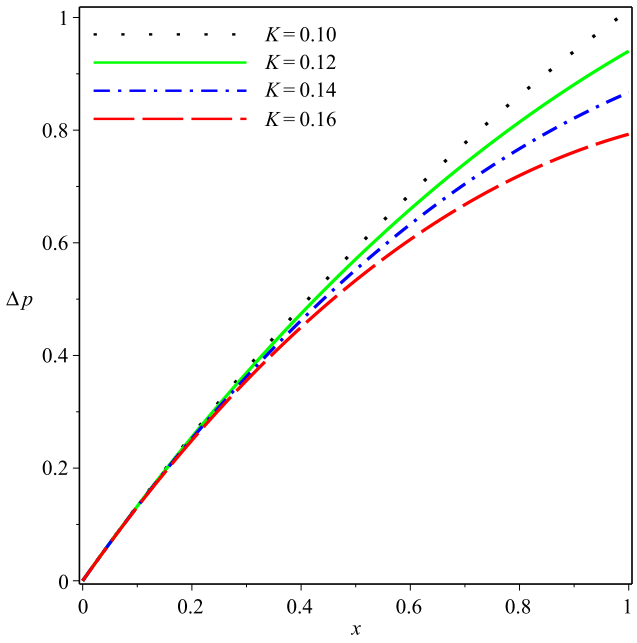

Figure 10. Effect of K on the mean pressure drop for $p_i = 3$, $\lambda_1 = 0.1$, $\lambda_2 = 0.03$.

A similar approach can be adopted to evaluate the expression for calculation of mean pressure drop in FPD between $x = 0$ and $x = L$. By using Eq. (58) the following expression can be obtained for the mean pressure drop in a flat plate hemodialyzer

$$\begin{aligned}\Delta p(1) &= \overline{p}(0) - \overline{p}(1),\\ &= p_i + \frac{\xi}{10AK}(5 - \lambda_2 K p_i)\sinh\xi + \frac{\xi p_i \lambda_2}{5A}\sinh 2\xi\\ &\quad + \frac{1}{20A^2(1+\lambda_1)}[3\lambda_2 + (4A^2 K p_i^2 \lambda_2 - 20A^2 p_i)(1+\lambda_1)]\cosh\xi\\ &\quad - \frac{\lambda_2}{20A^2(1+\lambda_1)}[3 + 4A^2 K p_i^2 (1+\lambda_1)]\cosh 2\xi.\end{aligned} \tag{67}$$

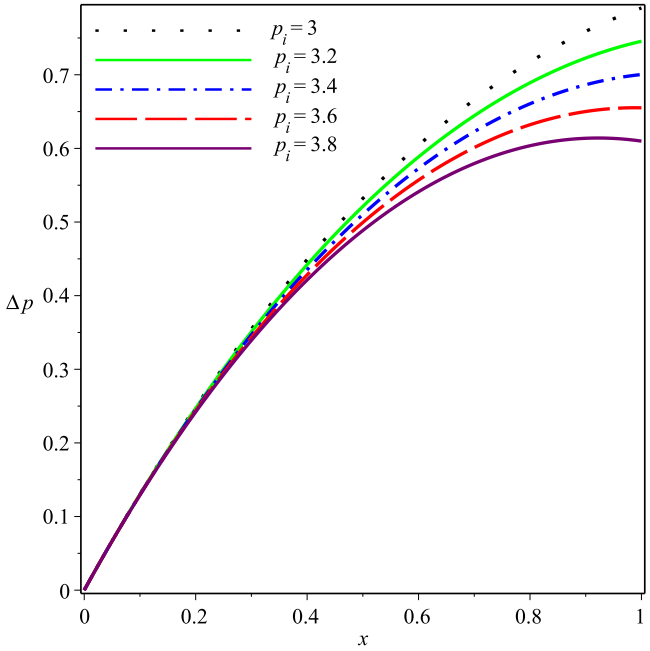

Figure 11. Effect of p_i on the mean pressure drop for $K = 0.16$, $\lambda_1 = 0.1$, $\lambda_2 = 0.03$.

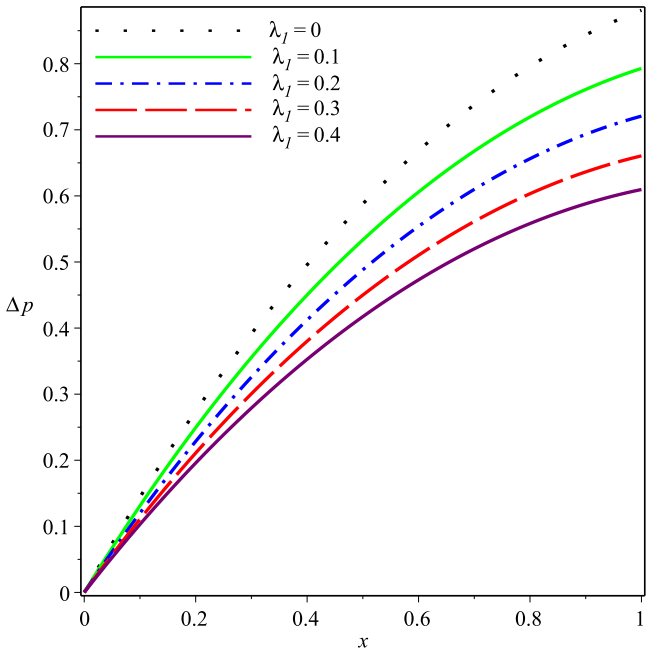

Figure 12. Effect of λ_1 on the mean pressure drop for $p_i = 3$, $K = 0.16$, $\lambda_2 = 0.03$.

For checking the accuracy of these expressions, we are employing the experimental data provided in[5,29] as shown in Table 1. This data corresponds to a disposable flat-plate artificial kidney and is also referred to as the data for an RP kidney. By substituting these parameters in Eq. (66) along with $\lambda_1 = 0.1$ and $\lambda_2 = 0.03$[21–23] results in an equation with one variable K. By expanding the hyperbolic functions in this equation in the power series of K up to $O(K^3)$ and then solving the resulting equation we obtain a real root $K = 6.23 \times 10^{-4}$. The ultrafiltration coefficient L_p is then computed from $K = \frac{L_p L^2}{a^3 t}$. This results in $L_p = 6.66 \times 10^{-16}\,\mathrm{cm}^2$ (see Table 2).

In a similar way by substituting $K = 6.23 \times 10^{-4}$ and the parameters given in Table 1 along with $\lambda_1 = 0.1$ and $\lambda_2 = 0.03$ in Eq. (67), mean pressure drop in an FPD can be computed. This results in the mean pressure drop $\overline{p}(0) - \overline{p}(L) = 11.5\,\mathrm{mm\ Hg}$ (see Table 2).

In the data for membranes of hemodialyzer, filtration coefficient L_p value is usually not given. Results of experiments performed by Kaufmann *et al.*[30] show that at the normal body temperature regenerated cellulose

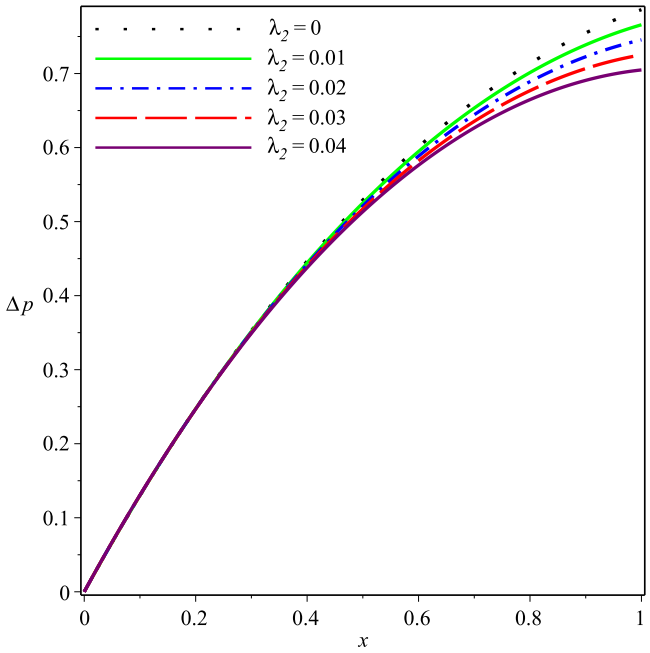

Figure 13. Effect of λ_2 on the mean pressure drop for $p_i = 3$, $K = 0.16$, $\lambda_1 = 0.1$.

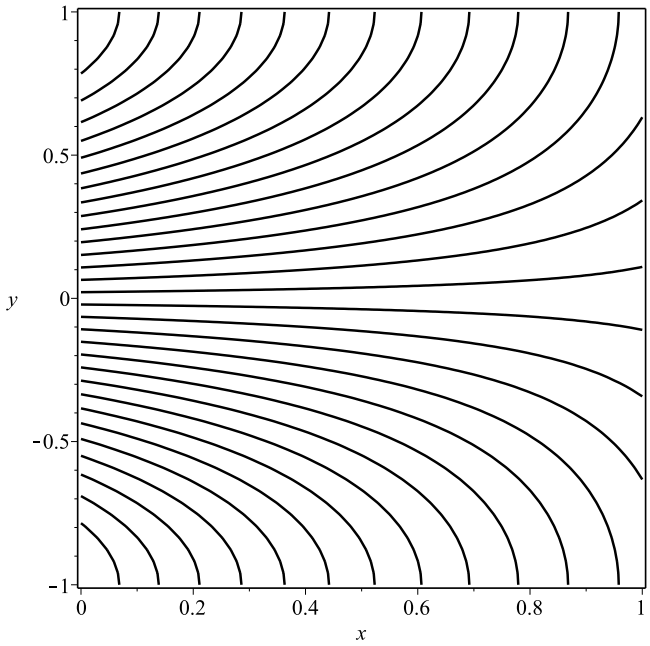

Figure 14. Streamline pattern of the flow or $p_i = 3$, K = 0.16, $\lambda_1 = 0.1$, $\lambda_2 = 0.03$.

has the hydraulic permeability equal to 2.41×10^{-11} cm^3/dynes-sec when the membrane has a thickness equal to 7.5×10^{-3} cm. Taking the fluid viscosity equal to 6.9×10^{-3} dynes-sec/cm^2 from Table 1, this results in $L_p = 1.25 \times 10^{-15}$ cm^2. The ultrafiltration coefficient computed by the empirical results of Marshall *et al.*[5] shows that $Lp = 6.36 \times 10^{-16}$ cm^2. It is also revealed in the experiments discussed in[5,29] that the mean pressure drop in an FPD is approximately 15 mm Hg. Thus a good agreement between the presented and earlier obtained experimental and empirical values of the ultrafiltration coefficient and mean pressure drop is found. This builds a confidence in stating that the presented model can be used to obtain theoretical results in advance to study the hydrodynamical aspects of the flow in a flat plate hemodialyzer.

Graphs of the ultrafiltration rate Q_A versus p_i, K and A are plotted in Figs 18–20, for fixed values of other parameters. These graphs state that Q_A depends linearly on p_i, or alternatively the ultrafiltration rate is linearly dependent on the trans-membrane pressure difference $\overline{p}(0) - p_m$. It is also evident from these graphs that Q_A is

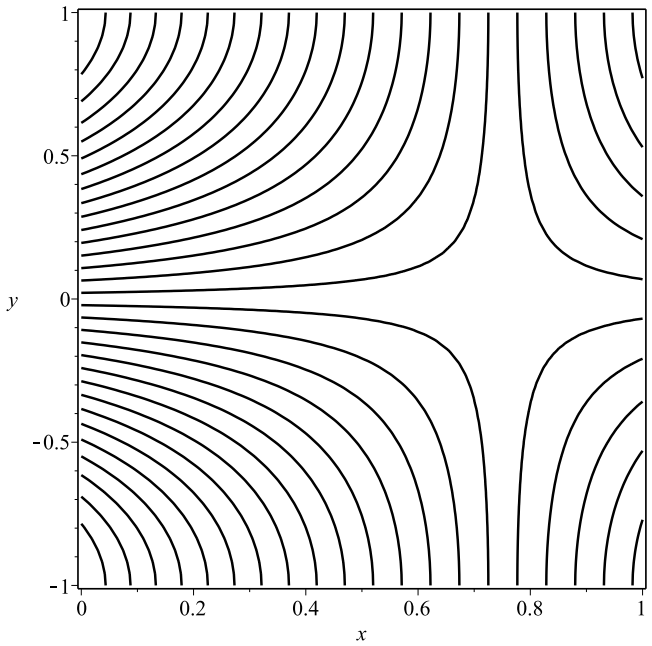

Figure 15. Streamline pattern of the flow for $p_i = 3$, $K = 0.25$, $\lambda_1 = 0.1$, $\lambda_2 = 0.03$.

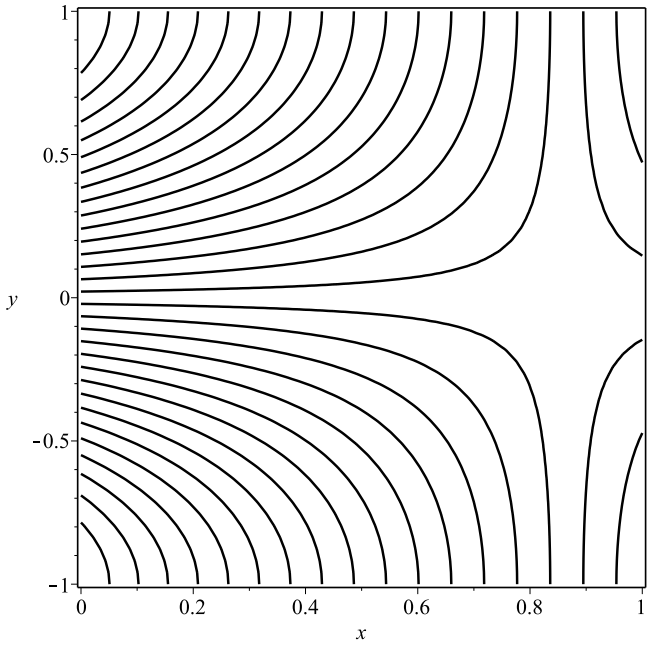

Figure 16. Streamline pattern of the flow for $p_i = 4$, $K = 0.16$, $\lambda_1 = 0.1$, $\lambda_2 = 0.03$.

directly proportional to the dimensionless filtration coefficient K. Expressions for the dimensionless parameters and Fig. 19 also reveal that the ultrafiltration rate is directly proportional to the mechanical filtration coefficient L_p and membrane area, and is inversely proportional to the membrane thickness and channel half width. Dependence of the ultrafiltration rate on the dimensionless filtration coefficient is also presented in Table 3. The linear dependence of Q_A on $\bar{p}(0) - p_m$ have been found experimentally by Malino *et al.*[31] and Mcdonald[32]. A series of experiments performed by Brown *et al.*[33] also highlights the dependence of Q_A on the mechanical filtration coefficient, membrane thickness and the membrane area.

For a given or desired mechanical filtration coefficient L_p, Eq. (66) can also be used to determine the magnitude of membrane thickness. This fact is explained in Fig. 21 which shows the behavior of dimensionless ultrafiltration rate Q_A with the trans-membrane pressure difference for different values of membrane thickness. The experimental curve in this graph is plotted by admitting the experimental result of Kauffmann *et al.*[30] which

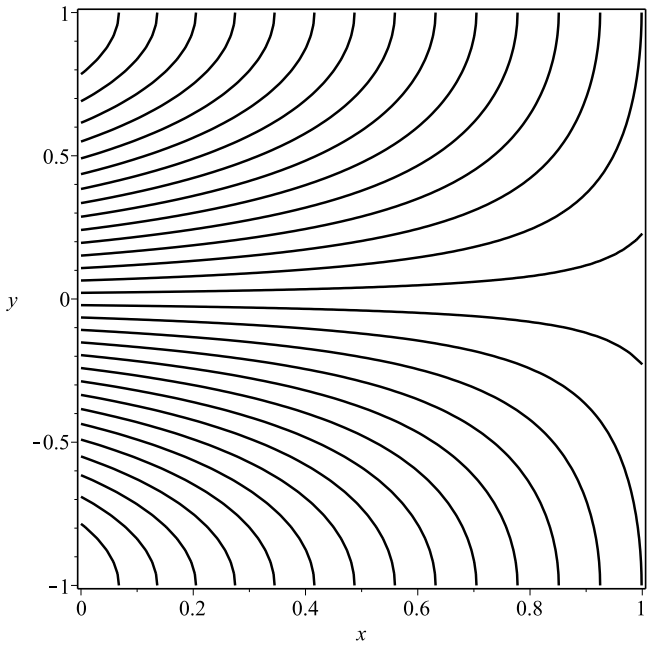

Figure 17. Streamline pattern of the flow for $p_i = 3$, $K = 0.16$, $\lambda_1 = 2$, $\lambda_2 = 0.03$.

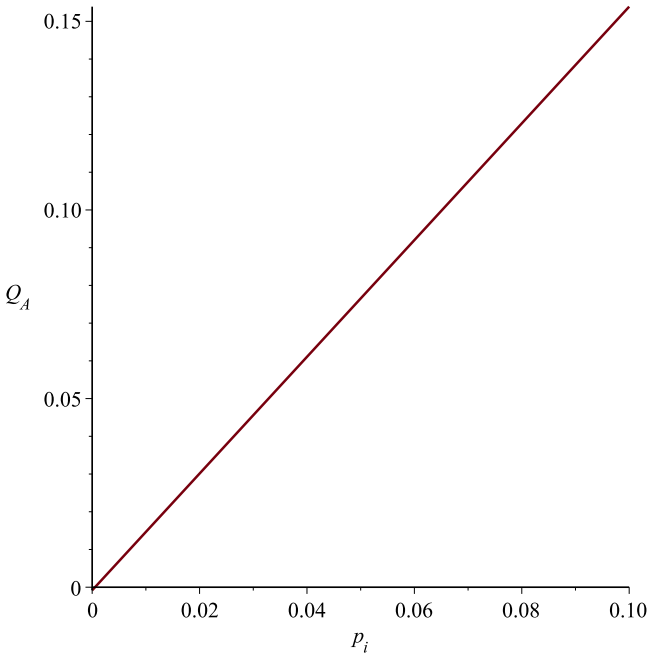

Figure 18. Ultrafiltration rate versus p_i, $K = 0.0006$, $A = 1288$.

Parameter	Abbreviation	Numerical Value
Mechanical filtration coefficient	L_p	$6.66 \times 10^{-16}\,\mathrm{cm}^2$
Dimensionless Mechanical filtration coefficient	K	6.23×10^{-4}
Mean pressure drop	$\bar{p}(0) - \bar{p}(L)$	11.55 mm Hg

Table 2. Computed values for the proposed Jeffrey fluid model.

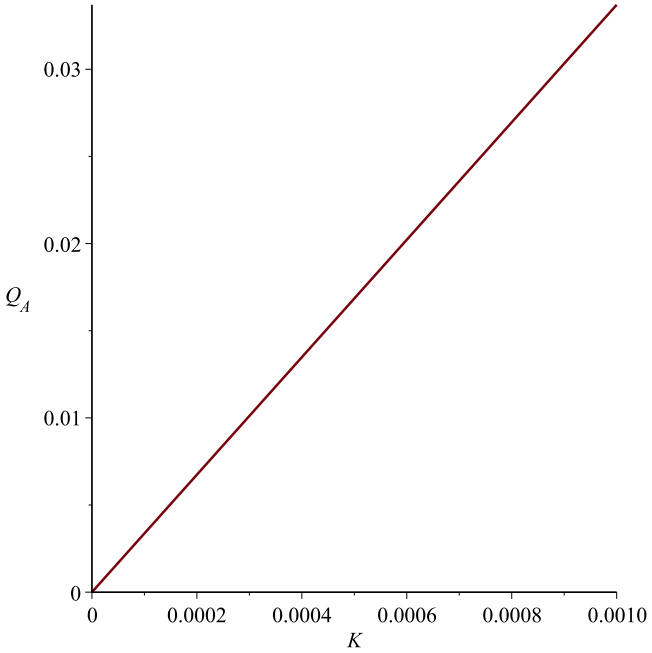

Figure 19. Ultrafiltration rate versus K, $p_i = 0.013$, $A = 1288$.

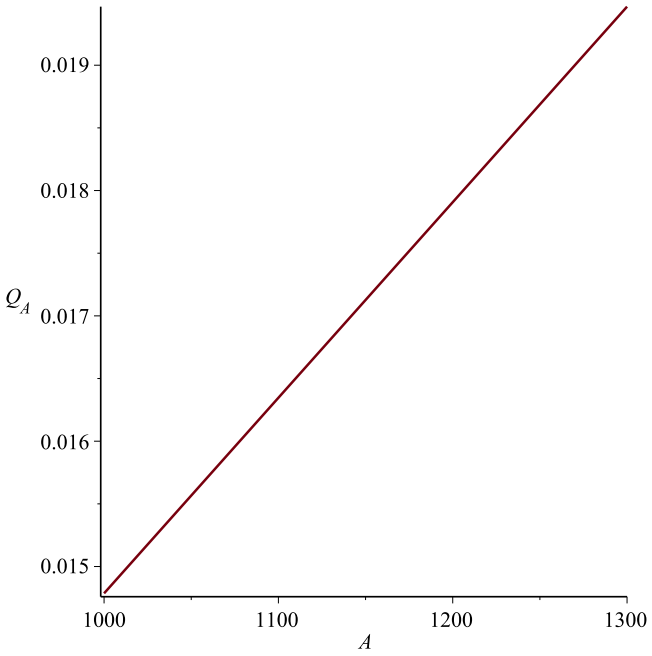

Figure 20. Ultrafiltration rate versus A, $p_i = 0.013$, $K = 0.0006$.

Wall Permeability	0.008	0.010	0.012	0.014	0.016	0.018
Ultrafiltration Rate	0.40	0.50	0.60	0.70	0.80	0.91

Table 3. Dimensionless ultrafiltration rate in a flat plate hemodialyzer.

states that L_p is $1.25 \times 10^{-15}\,\mathrm{cm}^2$. From this figure it can be seen that for experimental and theoretical curves to be in good agreement, the membrane thickness t should be approximately $1.5.0 \times 10^{-3}\,cm$. This thickness is approximately half of the estimated thickness obtained from the data of Funck-Bretano *et al.*[29]. The importance of membrane thickness in determining the ultrafiltration rate can also be seen from this graph. For example, it

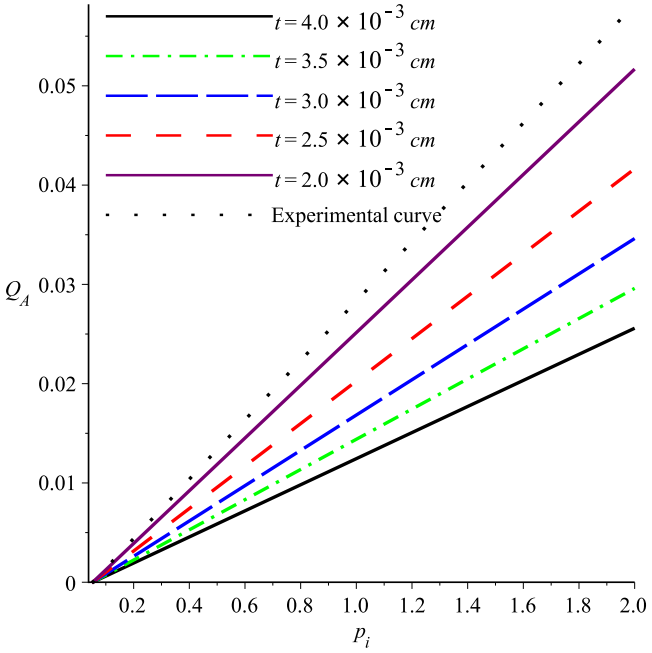

Figure 21. Ultrafiltration rate versus p_i for different membrane thicknesses.

can be seen that magnitude of the ultrafiltration rate can be doubled if the membrane thickness is halved. In order to determine a desired ultrafiltration rate for variations of the dimensionless filtration coefficient K, theoretical values of the ultrafiltration rate are tabulated in Table 3. It can be seen that increase in K causes the higher ultrafiltration rate.

Conclusions

The Jeffrey fluid model is a simpler model that describes well the physiological flows of non-Newtonian nature. In the study of fluid flow problems in porous-walled channels of small width, the presented model can serve as generalization of the usual Newtonian fluid model, since the obtained results can be reduced to the later one's by substituting parameters λ_1 and λ_2 equal to zero. The derived equations for the ultrafiltration rate and the mean pressure difference can be confidently used in studying the flow in a flat plate hemodialyzer. In applying the current results to study the problem of flow in flat plat hemodialyzer, one should not overlook the physical aspects of the flow phenomenon. It is also concluded the presented results are theoretical in their soul, therefore one should perform more experimental and theoretical investigation in order to have a complete understanding of the flow in a flat plat hemodialyzer.

Received: 8 April 2019; Accepted: 16 October 2019;
Published online: 04 November 2019

References

1. Nikolay Voutchkov. *Desalination engineering: planning and design*. McGraw Hill Professional (2012).
2. Macey, R. I. Pressure flow patterns in a cylinder with reabsorbing walls. *The bulletin of mathematical biophysics* **25**(1), 303–312 (1963).
3. Macey, R. I. Hydrodynamics in the renal tubule. *The Bulletin of mathematical biophysics* **27**(2), 117–124 (1965).
4. Marshall, E. A. & Trowbridge, E. A. Flow of a newtonian fluid through a permeable tube: the application to the proximal renal tubule. *Bulletin of mathematical biology* **36**(5–6), 457–476 (1974).
5. Marshall, E. A., Trowbridge, E. A. & Aplin, A. J. Flow of a newtonian fluid between parallel flat permeable platesthe application to a flat-plate hemodialyzer. *Mathematical Biosciences* **27**(1–2), 119–139 (1975).
6. Kahshan, M., Lu, D. & Rahimi-Gorji, M. Hydrodynamical study of flow in a permeable channel: Application to flat plate dialyzer. *International Journal of Hydrogen Energy* **44**(31), 17041–17047 (2019).
7. Papanastasiou, T. C. *et al. VISCOUS FLUID FLOW*. CRC Press LLC, Florida (2000).
8. Abraham, S. Berman. *Laminar flow in channels with porous walls. Journal of Applied Physics* **24**(9), 1232–1235 (1953).
9. Sellars, J. R. Laminar flow in channels with porous walls at high suction reynolds numbers. *Journal of Applied Physics* **26**(4), 489–490 (1955).
10. Yuan, S. W. Further investigation of laminar flow in channels with porous walls. *Journal of Applied Physics* **27**(3), 267–269 (1956).
11. Kozinski, A. A., Schmidt, F. P. & Lightfoot, E. N. Velocity profiles in porous-walled ducts. *Industrial & Engineering Chemistry Fundamentals* **9**(3), 502–505 (1970).
12. Siddiqui, A. M., Haroon, T. & Shahzad, A. Hydrodynamics of viscous fluid through porous slit with linear absorption. *Applied Mathematics and Mechanics* **37**(3), 361–378 (2016).
13. Ahmad, S., Nadeem, S. & Muhammad, N. Boundary layer flow over a curved surface imbedded in porous medium. *Communications in Theoretical Physics* **71**(3), 344 (2019).
14. Noor Muhammad, S., Nadeem & Mustafa, M. T. Hybrid isothermal model for the ferrohydrodynamic chemically reactive species. *Communications in Theoretical Physics* **71**(4), 384 (2019).

15. Muhammad, N., Nadeem, S. & Mustafa, M. T. T. Impact of magnetic dipole on a thermally stratified ferrofluid past a stretchable surface. *Proceedings of the Institution of Mechanical Engineers, Part E: Journal of Process Mechanical Engineering* **233**(2), 177–183 (2019).
16. Muhammad, N., Nadeem, S. & Mustafa, M. T. Analysis of ferrite nanoparticles in the flow of ferromagnetic nanofluid. *PloS one* **13**(1), e0188460 (2018).
17. Nadeem, S., Raishad, I., Muhammad, N. & Mustafa, M. T. Mathematical analysis of ferromagnetic fluid embedded in a porous medium. *Results in physics* **7**, 2361–2368 (2017).
18. Nadeem, S., Ahmad, S. & Muhammad, N. Computational study of falkner-skan problem for a static and moving wedge. *Sensors and Actuators B: Chemical* **263**, 69–76 (2018).
19. Nadeem, S., Ahmad, S., Muhammad, N. & Mustafa, M. T. Chemically reactive species in the flow of a maxwell fluid. *Results in physics* **7**, 2607–2613 (2017).
20. R. B Bird *et al. DYNAMICS OF POLYMERIC LIQUIDS, Volume 1*. JOHN WILEY & SONS, New York (1987).
21. Tasawar, H. & Ali, N. Peristaltic motion of a jeffrey fluid under the effect of a magnetic field in a tube. *Communications in Nonlinear Science and Numerical Simulation* **13**(7), 1343–1352 (2008).
22. Nadeem, S. & Akram, S. Peristaltic flow of a jeffrey fluid in a rectangular duct. *Nonlinear Analysis: Real World Applications* **11**(5), 4238–4247 (2010).
23. Nallapu, S. & Radhakrishnamacharya, G. Jeffrey fluid flow through porous medium in the presence of magnetic field in narrow tubes. *International Journal of Engineering Mathematics*, **2014** (2014).
24. Radhakrishnamacharya, G., Peeyush, C. & Kaimal, M. R. A hydrodynamical study of the flow in renal tubules. *Bulletin of mathematical biology* **43**(2), 151–163 (1981).
25. Palatt, P. J., Sackin, H. & Tanner, R. I. A hydrodynamic model of a permeable tubule. *Journal of theoretical biology* **44**(2), 287–303 (1974).
26. Siddiqui, A. M., Haroon, T. & Kahshan, M. MHD flow of newtonian fluid in a permeable tubule. *Magnetohydrodynamics* **51**(4), 655–672 (2015).
27. Lu, D., Kahshan, M. & Siddiqui, A. M. Hydrodynamical study of micropolar fluid in a porous-walled channel: Application to flat plate dialyzer. *Symmetry*, **11**(4), (2019).
28. Drukker, W., Parsons, F. M. & Maher, J. F. *Replacement of renal function by dialysis: a textbook of dialysis*. Springer Science & Business Media (2012).
29. Funck-Brentano, J. L. *et al*. A new disposable plate-kidney. *ASAIO Journal* **15**(1), 127–130 (1969).
30. Kaufmann, T. G. & Leonard., E. F. Studies of intramembrane transport: A phenomenological approach. *AIChE Journal* **14**(1), 110–117 (1968).
31. Malinow, M. R. & Korzon, W. An experimental method for obtaining an ultrafiltrate of the blood. *Translational Research* **32**(4), 461–471 (1947).
32. McDonald, H. P. Jr. An automatic peritoneal dialysis machine: preliminary report (1966).
33. Brown, H. W. & Schreiner, G. E. Prolonged hemodialysis with bath refrigeration: the influence of dialyzer membrane thickness, temperature and other variables on performance. *Trans Am Soc Artif Intern Organs* **8**(1), 187–194 (1962).

Acknowledgements

This work was supported by China Postdoctoral Science Foundation (Nos. 2019M651715).

Author contributions

Muhammad Kahshan performed mathematical modeling, numerical simulation and write up of the article. The work was supervised and reviewed by Prof. D. Lu and Prof. A.M. Siddiqui.

Competing interests

The authors declare no competing interests.

Additional information

Correspondence and requests for materials should be addressed to D.L.

Reprints and permissions information is available at www.nature.com/reprints.

Publisher's note Springer Nature remains neutral with regard to jurisdictional claims in published maps and institutional affiliations.